IEEE Access
Multidisciplinary | Rapid Review | Open Access Journal

Received December 27, 2019, accepted January 7, 2020, date of publication January 13, 2020, date of current version January 27, 2020.

Digital Object Identifier 10.1109/ACCESS.2020.2966280

Large Dynamic Range and High Sensitivity PGC Demodulation Technique for Tri-Component Fiber Optic Seismometer

CHANGBO HOU[1,2], GUOWEI LIU[1], SHUAI GUO[1], SHUAIFEI TIAN[2], AND YONGGUI YUAN[2]

[1]College of Information and Communication Engineering, Harbin Engineering University, Harbin 150001, China
[2]College of Physics and Optoelectronic Engineering, Harbin Engineering University, Harbin 150001, China

Corresponding author: Yonggui Yuan (yuanyonggui@aliyun.com)

This work was supported in part by the Natural Science Foundation of Heilongjiang Province under Grant LH2019F005 and in part by the Fundamental Research Funds for the Central Universities under Grant HEUCFJ180801, Grant HEUCF180801, Grant 3072019CF0801, and Grant 3072019CFM0802.

ABSTRACT Three-component fiber optic seismometers are widely used in the detection of seismic signals. The arctangent approach of phase-generated carrier (PGC-Arctan) demodulation algorithm is one of the commonly used demodulation techniques in FOISs. Nonlinear factors such as phase modulation depth(C) variation and light intensity disturbance (LID) have an important impact on performance of traditional PGC demodulation algorithms. This paper introduces a new demodulation algorithm called Kalman filtering ellipse (PGC-Arctan-EKF) demodulation algorithm, which can improve the robustness of the fitting. In order to meet the requirements of high performance and low power consumption of seafloor sensing, Tri-Component fiber optic seismometer based on SoC(ARM +FPGA) is proposed in this paper. The phase self-noise of the system is better than −115 dB re rad /$Hz^{1/2}$,and the large signal can reach 66 dB re rad/$Hz^{1/2}$ @220Hz with the THD is −61.22 dB.

INDEX TERMS Tri-component fiber optic seismometer, PGC-arctan-EKF, ellipse fitting, SoC.

I. INTRODUCTION

Earthquake monitoring and early warning are of great significance for reducing property damage and casualties caused by earthquakes. As the forefront of the seismic monitoring system, the seismometer is directly related to the reliability of the entire seismic network and plays an important role.

In the new generation of geophones, the fiber optic seismic detector has the advantages of a passive sensor, strong anti-electromagnetic interference, high sensitivity, small footprint, easy network deployment, etc. Japan [1], [2], the United States [3], and Canada [4] have deployed experimental fiber-optic interferometers in submarine seismic observation networks last few years. While these studies have achieved some good results, they also reveal some areas to improve the stability of these systems. Among them, one of the main problems faced by fiber optic seismometers is the design of probes and demodulation systems with large dynamic range and high sensitivity.

The associate editor coordinating the review of this manuscript and approving it for publication was Guan Gui.

Due to the advantages of wide dynamic range, high linearity and sensitivity, high precision of phase measurement and multiplexing of sensors, PGC demodulation scheme has been widely used in fiber optic seismometer [5]–[16]. PGC-Arctan is a relatively common type of PGC demodulation schemes, while nonlinear distortion has a greater impact on the results of PGC demodulation systems [17]–[23].

In the process of solving the nonlinear distortion problem in PGC demodulation, many scholars have proposed effective methods [24]–[28]. He *e*t al. [29] presented a algorithm based on arctangent function and differential-self-multiplying-integrate of PGC demodulation algorithm (DSM), this method can suppress nonlinear distortion within a certain drift range of C value [29]. Zhang and Li [30] proposed an interference sensor based on DSM, which eliminates the influence of modulation depth C on the demodulation result, but the dynamic range is limited [30]. Chen *e*t al. [31] proposed and tested a three-component detector based on Michelson's interferometry. The system has an average system noise level of −123.55 re rad /$Hz^{1/2}$, ranging from 0 Hz to 500 Hz, and the dynamic range of over

116 dB [31], [32].Then Tong *et* al. [22] proposed a new algorithm, which could eliminate the interference of light intensity and the influence caused by the fluctuation of environment. This method introduced the carrier's third harmonic and high-pass filter, however the computation of this method was very complicated and difficult to be implemented by hardware [22]. In recent years, Ni *et* al. [33] introduced the EFA to compensate for nonlinear errors caused by light source noise, C-value fluctuations, and carrier phase delay. However, the algorithm requires the measured signal changing greater than $\pi/2$ rad, otherwise it will result in increased error in the demodulation results [33]. All of the above methods improve the measurement accuracy of the system by introducing nonlinear error correction, however, there are still many shortage to be improved for practical subsea fiber optic sensing applications.

This paper proposes a algorithm called Tri-component-PGC-Arctan-EKF demodulation algorithm based on Xilinx MPSoC. The Kalman filtering algorithm is introduced to suppress nonlinear distortion. At the same time, this paper further optimizes the algorithm to facilitate deployment on hardware with limited resources.

The structure of this paper is as follows. In section 2, the overall configuration of the system and the specific form of the demodulated signal are introduced. In section 3, the specific demodulation method and the overall flow of its PGC-Arctan-EKF are introduced. The experimental results and discussion are presented in section 4. In section 5, the conclusion is given.

II. SYSTEM CONFIGURATION

The system configuration of the tri-component fiber optic seismometer based on Xilinx MPSoC is shown in Fig. 1. In the PGC modulation part, the carrier signals generated by four channels DAC modulate the interference signal through PZT modulator. Then the output optical signals of Mach-Zehnder interferometer are converted into electrical signals by photoelectric conversion board. In the PGC modulation part, the sampled digital signals by high-speed ADC are demodulated by the real-time demodulation module on the FPGA. Finally, the demodulated output signals are transmitted directly to the server for storage and recording via the network.

The laser source is a single-frequency laser (RIO ORION Laser Module, RIO) with the wavelength of 1550.11 nm. The combined phase modulation introduced by a PZT. And the signal processing card is an self-developed board card, based on a SOC (Zynq7100, Xilinx), with a FPGA and a ARM Cortex-A9 MPCore, i.e. In addition, the data acquisition board is also an self-developed board card which integrates high-speed ADC and DAC with 16 bits resolutions, which the sampling rate can reach 100MSPS and 500MSPS respectively.

The interference signal [31], [32] can be expressed by

$$I(t) = A + B\cos[C\cos\omega_0 t + \varphi(t)] \tag{1}$$

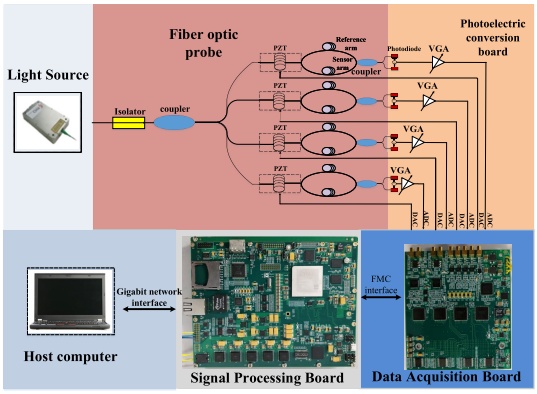

FIGURE 1. System configuration for Tri-Component Fiber Optic seismometer based on Xilinx MPSoC.

In equation (1), A represents the direct current component of the light intensity after the interference, and B is the alternating current component of the light intensity after the interference. C is the phase modulation depth. $\cos\omega_o t$ is the local carrier signal. $\varphi(t)$ represents the collected phase signal. In the actual environment, there is some deviation from the actual signal due to noise interference and the influence of the system.

III. THE PRINCIPLE AND PROCESSES OF PGC-ARCTAN-EKF

The principle and processes of PGC-Arctan-EKF is shown in Figure 2. The algorithm consists of a nonlinear error suppression module and a fringe subdivision module. Because it is not suitable for complicated mathematical operations in FPGA, the CORDIC algorithm is used to simplify the calculation process and save calculation resources.

Multiplying the equation (1) with the local carrier signals $\varphi_o(t) = C\cos\omega_0 t$ and its second-harmonic carrier $\varphi_o(2t) = C\cos 2\omega_0 t$ respectively to obtain a mixed signals, and each is filtered by a low-pass filter.Then a pair of non-strict orthogonal signals $I_x(t)$ and $I_y(t)$ can be obtained

$$I_x(t) = -BJ_1(C)\sin(\varphi_s(t)) \tag{2}$$

$$I_y(t) = -BJ_2(C)\cos(\varphi_s(t)) \tag{3}$$

where $\varphi_s(t)$ is the acquired phase signal,and dividing $J_1(C)$ and $J_2(C)$ yields

$$I_{div}(t) = \frac{J_1(C)}{J_2(C)}\tan\varphi(t) \tag{4}$$

In equation(4),$J_1(C)$ and $J_2(C)$ are the Bessel functions of C value. Then calculating the demodulation phase by arctangent as shown in equation(5)

$$\varphi(t) = \arctan\left[\frac{J_2(C)}{J_1(C)}I_{div}(t)\right] \tag{5}$$

Taking the value of C as 2.63 rad,which can make $J_1(C)$ and $J_2(C)$ almost equal. At this point, the impact on the demodulation results is basically minimal.

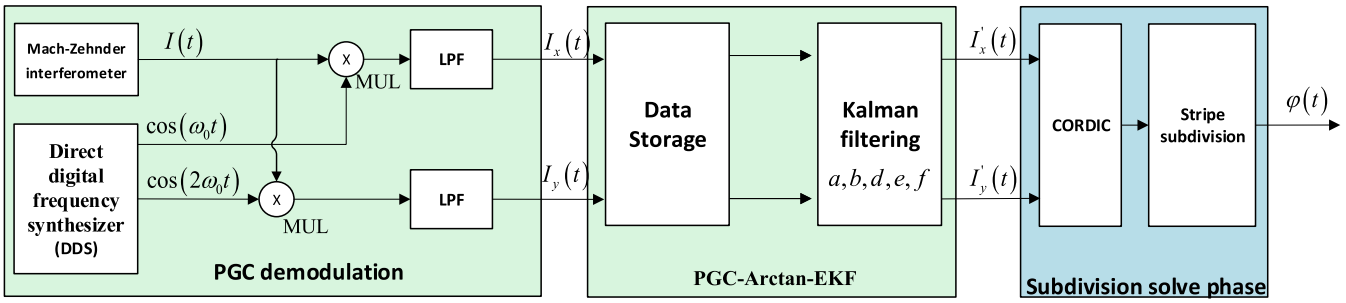

FIGURE 2. PGC-Arctan-EKF algorithm. MUL: multiplier. LPF: low pass filter. a, b, d, e, f: ellipse parameters.

A. THE PRINCIPLE OF KALMAN FILTERING

Kalman filtering can be used to estimate parameters. And the system model needs to be constructed at first. The general curve equation of the ellipse can be expressed by:

$$f(x, y) = ax^2 + 2bxy + cy^2 + 2dx + 2ey + f = 0 \quad (6)$$

where $a + c > 0$,and in order to avoid solving the equation to get hyperbola, the elliptic equation should be normalized. And the normalization condition is:

$$a + c = 1 \quad (7)$$

In order to ensure that each parameter value of the ellipse is valid, $f = 1$ is not used to center the ellipse in the above formula, because each parameter of the ellipse is too small when $f = 1$, it will cause calculation errors.Meanwhile the ellipse passing through the origin cannot be included. The parameters of the ellipse are represented by a five-dimensional vector:

$$\boldsymbol{X} = (a, b, d, e, f)' \quad (8)$$

Estimating the vector and taking the points to be fitted in the system as the observations which used in the estimation. The points to be fitted can be expressed as:

$$\boldsymbol{N_i} = (x_i, y_i)' \quad (9)$$

where the deviation between the observed data and the real data is:

$$\boldsymbol{v_i} = \boldsymbol{Y_i} - \boldsymbol{N_i} \quad (10)$$

The $\boldsymbol{v_i}$ in the equation(11) represents Gaussian noise, and the covariance matrix of the corresponding noise is:

$$cov\,[\boldsymbol{v_i}] = \boldsymbol{R_i} \quad (11)$$

For each point to be fitted, the ellipse equation is a non-linear constraint. The parameters to be measured and the points to be estimated are substituted as the observation equation:

$$F(\boldsymbol{X_i}, \boldsymbol{Y_i}) = 0 \quad (12)$$

where $F(\boldsymbol{X_i}, \boldsymbol{Y_i}) = 0$ is the value when substituting the real parameters of the ellipse, and there is no deviation. When the estimated parameter $\boldsymbol{M}$ and the observed data $\boldsymbol{N}$ are given, the deviation can be obtained by substituting the data points to be fitted into the estimated elliptic equation is $F(M, N) \neq 0$.

Kalman filtering requires linearization of signals when applied to nonlinear systems. Substituting the estimated value $\boldsymbol{M_i}$ of the elliptic parameter $\boldsymbol{X_i}$ and the observation data $\boldsymbol{N_i}$ of $\boldsymbol{Y_i}$ into $F(\boldsymbol{X_i}, \boldsymbol{Y_i}) = 0$ and use Taylor series to linearize the non-linear function, the following formula can be obtained:

$$F(\boldsymbol{X_i}, \boldsymbol{Y_i}) = F(\boldsymbol{M_i}, \boldsymbol{N_i}) + [\nabla_X F(\boldsymbol{M_i}, \boldsymbol{N_i})'(\boldsymbol{X_i} - \boldsymbol{N_i})] + [\nabla_Y F(\boldsymbol{M_i}, \boldsymbol{N_i})'(\boldsymbol{Y_i} - \boldsymbol{N_i})] = 0 \quad (13)$$

The formula(14) also can be expressed as:

$$-F(\boldsymbol{M_i}, \boldsymbol{N_i}) = [\nabla_X F(\boldsymbol{M_i}, \boldsymbol{N_i})'(\boldsymbol{X_i} - \boldsymbol{N_i})] + [\nabla_Y F(\boldsymbol{M_i}, \boldsymbol{N_i})'(\boldsymbol{Y_i} - \boldsymbol{N_i})] \quad (14)$$

In formula(15), $F(\boldsymbol{M_i}, \boldsymbol{N_i})$ can represent the distance deviates from the ellipse. Assuming $\boldsymbol{M_i} = [aa, bb, dd, ee, ff]'$, for the system $-F(\boldsymbol{M_i}, \boldsymbol{N_i})$ can also be expressed as:

$$-F(\boldsymbol{M_i}, \boldsymbol{N_i}) = -(aax_i^2 + 2bbx_iy_i + ccy_i^2 + 2ddx_i + 2eey_i + ff) \quad (15)$$

Differentiating the formula(16) can get:

$$\nabla_X F(\boldsymbol{M_i}, \boldsymbol{N_i}) = (x_i^2 - y_i^2, 2x_iy_i, 2x_i, 2y_i, 1)' \quad (16)$$

$$\nabla_Y F(\boldsymbol{M_i}, \boldsymbol{N_i}) = 2(aax_i + bby_i + dd, bbx_i + ccy_i + ee)' \quad (17)$$

In general, the observation equation of the Kalman filter is:
Let $\Delta \boldsymbol{X} = \boldsymbol{X} - \boldsymbol{M}$ can get:
The deviation observations:

$$Z = -F(\boldsymbol{M_i}, \boldsymbol{N_i}) \quad (18)$$

The observation matrix:

$$H = \nabla_X F(\boldsymbol{M_i}, \boldsymbol{N_i}) \quad (19)$$

The observation noise:

$$\boldsymbol{v_i} = \nabla_Y F(\boldsymbol{M_i}, \boldsymbol{N_i})'(\boldsymbol{Y_i} - \boldsymbol{N_i}) \quad (20)$$

The observation noise expectation and the covariance matrix:

$$E[\boldsymbol{v_i}] = \nabla_Y F(\boldsymbol{M_i}, \boldsymbol{N_i})' E[(\boldsymbol{Y_i} - \boldsymbol{N_i})] = 0 \quad (21)$$

$$var[\boldsymbol{v_i}] = [\nabla_Y F(\boldsymbol{M_i}, \boldsymbol{N_i})] R [\nabla_Y F(\boldsymbol{M_i}, \boldsymbol{N_i})]' = 4[(aax_i + bby_i + dd)^2 + (bbx_i + ccy_i + ee)^2] \sum^2 I \quad (22)$$

Algorithm 1 Kalman Filtering Algorithm

1 Select five points from the data points to be fitted to obtain a set of five-ary algebraic equations;
2 Use the solution of the system of equations as the initial value of the ellipse parameter: $\boldsymbol{X_s}$;
3 Initialization state vector: $\Delta \boldsymbol{X}(0)= [0, 0, 0, 0, 0]^T$;
4 The Kalman filter is used to fit the data points, and update the state vector and the state covariance matrix continuously;
5 The new parameters are added to the initial parameter estimates to get the estimated results for the new ellipse parameters;
6 Update the initial parameters each time and repeat (3)-(5);
7 When the results change in two adjacent estimates are less than the given error 10^{-8} during the update processing, it is considered to reach a convergence state, and the iteration is stopped.;

B. THE PRINCIPLE OF STRIPE SUBDIVISION ALGORITHM

For guaranting phase demodulation range of PGC-Arctan, the CORDIC algorithm based on stripe subdivision algorithm is introduced in this paper.

The two orthogonal signals obtained after Kalman filtering can be expressed by the following formula

$$\begin{aligned} I_x &= \sin(\varphi(t)) \\ I_y &= \cos(\varphi(t)) \end{aligned} \tag{23}$$

It can be seen from the above equation that the signal $\varphi(t)$ to be measured can be obtained by performing the CORDIC algorithm, but the range of the signal solved by the CORDIC algorithm is $[-\pi, \pi]$, and it do not represent the true signal $\varphi(t)$ to be measured. The phase signal solved by the CORDIC algorithm is different from the actual signal by $2n\pi$.

As can be seen from Figure 3, when the signal demodulated by the CORDIC algorithm passes through the X-axis counterclockwise each time, the demodulated signal needs to add 2π to be the actual value of the demodulation signal. When the signal demodulated by the CORDIC algorithm passes clockwise through the X-axis, the demodulated signal needs to be subtracted by 2π to be the actual value of the demodulation signal. Thereby realizing the counting and arguing function of periodic stripes.

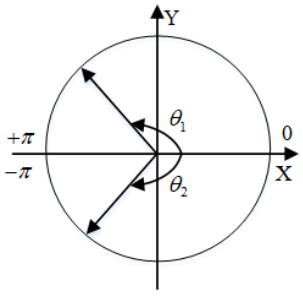

FIGURE 3. Stripe subdivision algorithm phase diagram.

C. REALIZATION OF THE PGC DEMODULATION FOR TRI-COMPONENT FIBER OPTIC SEISMOMETER

The general flow chart of signal processing for Tri-Component Fiber Optic seismometer based on FPGA + ARM is shown in Figure 4. FPGA includes lots of programmable logics, such as 444k logic cells and 2020 DSP Slices. These DSP Slices are able to complete multiplication in parallel within one clock, which can greatly improve the efficiencies of Kalman filtering and LPFs. The algorithm is implemented by HLS in FPGA, which is beneficial to the solution of Kalman filtering equations.

In order to reduce the consumption of hardware resources, digital filter, Kalman filtering are all time-division multiplexing. The basic steps of the computational procedure are as follows:

Firstly, four-channel interference signals are respectively converted into digital signals after sampling by high-speed ADC, which are expressed $S_1(t), S_2(t), S_3(t), S_4(t)$. The interference signals are separately multiplied with $\varphi_o(t) = C\cos\omega_0 t$ and $\varphi_o(2t) = C\cos 2\omega_0 t$. After filtering out the high-frequency components by Multi-Channel FIR, then two signals $I_{xi}(t)$ and $I_{yi}(t)$ that are non-strict orthogonal to each other can be obtained.

Secondly,the four non-strict orthogonal components $I_{xi}(t)$ and $I_{yi}(t)$ are corrected into orthogonal signals by EKF module. Initialization module are used to generate the state vector $\boldsymbol{X}$ and the covariance matrix $\boldsymbol{P}$ for Kalman filtering.In the process of Kalman filtering, the observation equation Z is established by the updated value at the last moment.In the prediction process of Kalman filtering, the state transition matrix $\boldsymbol{A} = I_1$, so the state prediction equation can be expressed as:

$$\boldsymbol{X}(\boldsymbol{k}|\boldsymbol{k}-\mathbf{1}) = \boldsymbol{X}(\boldsymbol{k}-\mathbf{1}) \tag{24}$$

Q is the covariance matrix of process noise w and the value $Q = 0$,so the state covariance prediction matrix can be expressed as:

$$\boldsymbol{P}(\boldsymbol{k}|\boldsymbol{k}-\mathbf{1}) = \boldsymbol{P}(\boldsymbol{k}-\mathbf{1}) \tag{25}$$

Then the parameters value are continuously updated according to the update equations.

Thirdly, it is sent to the next moment according to the state estimate and the error covariance estimate at time, and it enters the process of continuous iteration.

In the last, the four non-strict orthogonal components I'_{xi} and I'_{yi} can be calculated by solving KF equations module. And the I'_{xi} and I'_{yi} are extracted by CORDIC and subdivided by fringe to get the measured real phase signals.Then the four-channel demodulation phase signals are integrated and sent to ARM via HP AXI bus and then to the server via the network.

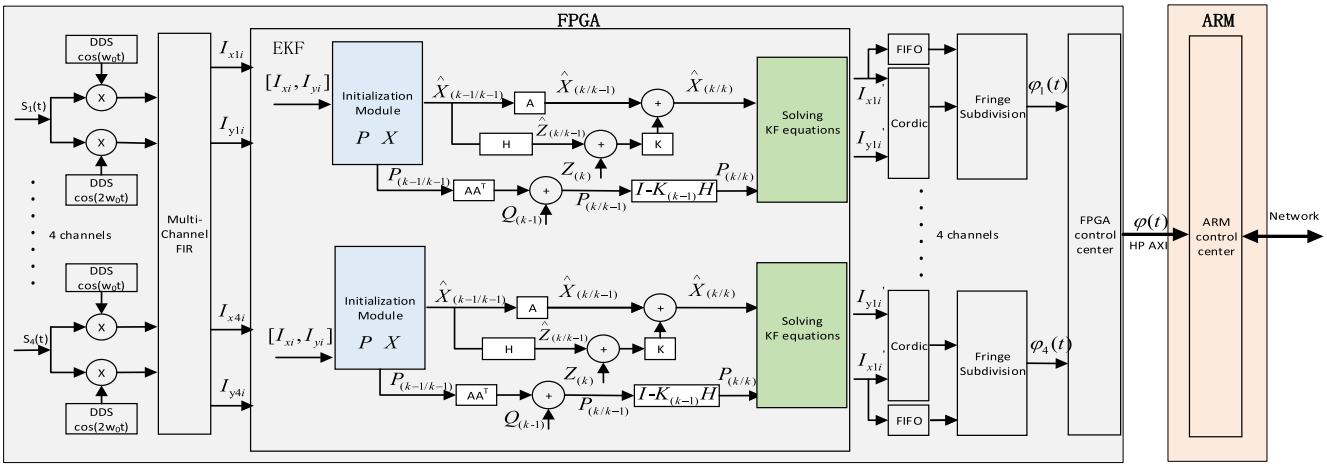

FIGURE 4. The general flow chart of signal processing for Tri-Component Fiber Optic seismometer. A:The state transition matrix. H:The observation matrix. K:The gain matrix.

IV. EXPERIMENTAL RESULTS AND ANALYSIS

The experimental results and analysis can be composed of the following 5 parts: the effectiveness of Kalman filtering, the minimum detectable signal level, the linearity of the system, the large signal response, and the channel crosstalk.

A. THE EFFECTIVENESS OF KALMAN FILTERING

As can be seen from Figure 5(a), due to the nonlinear distortion, the Lissajous figure of the two signals before the Kalman filtering is an ellipse, and the eccentricity of the ellipse after the Kalman filtering in Figure 5(b) are equal to 0,so the Lissajous image is a standard unit circle.

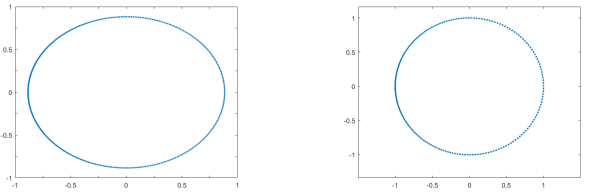

(a) The Lissajous figure before Kalman filtering

(b) The Lissajous figure after Kalman filtering

FIGURE 5. The effectiveness of Kalman filtering.

B. MINIMUM DETECTABLE SIGNAL LEVEL

The minimum detectable signal level of a fiber optic geophone system can be assessed by the phase self-noise of the system.Phase self-noise also marks the minimum value of the PGC demodulation system can demodulate. So it can be represented by the maximum of the phase self-noise power spectral density.

The test results are shown in Figure 6.In the above figure, ignoring the noise at low frequencies, it can be considered that the average value of the phase self-noise of the system from 0-2500 Hz is around -115.2 re rad /Hz$^{1/2}$. This means that the fiber geophone system has high sensitivity.

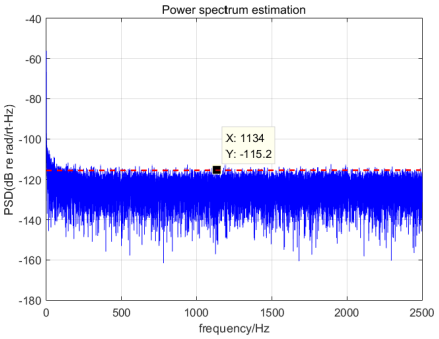

FIGURE 6. Noise of the geophone system output.

C. LINEARITY

Linearity is an important indicator for describing the static characteristics of a sensor, based on the assumption that the measured input is in a stable state. The linearity test scheme is shown in Figure 7. A certain signal is output through the Agilent signal, and it is added to the carrier signal by the adder then sent to the PZT. So the signal output from the demodula-

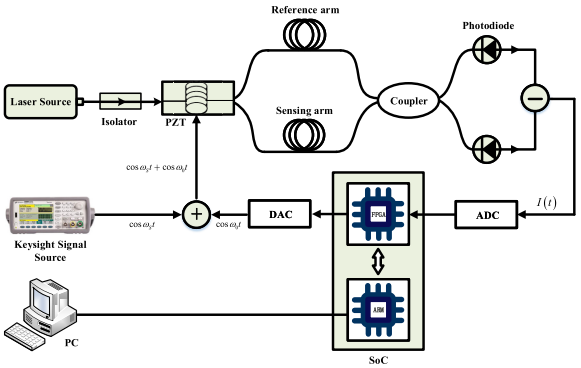

FIGURE 7. Linearity test scheme.

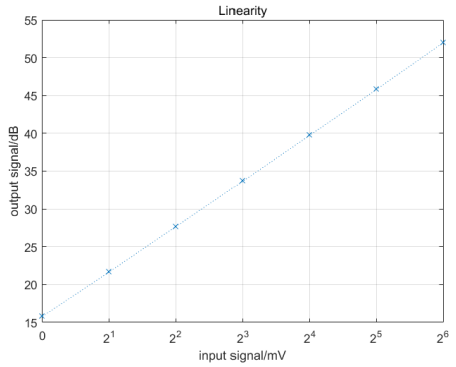

FIGURE 8. Linearity of the system.

tor can be measured. By changing the output amplitude of the signal source by 2 times, the size of the demodulated output signal should theoretically increase by 6.2dB.

As shown in Figure 8, according to the above conclusion, the results show that the designed fiber accelerometer has a good linear relationship.Substituting into equation (15)

$$\rho_{xy} = \frac{C_{ov}(X, Y)}{\sqrt{D(X)}\sqrt{D(Y)}} \tag{26}$$

the correlation coefficient is 0.998,it also can be seen that the linearity of the output signal is good.

D. LARGE SIGNAL RESPONSE

The large-signal response and phase self-noise together characterize the dynamic range of a fiber optic seismometer. The test method is shown in Figure 9,the optical fiber probe is placed on the vibration table, and the signal output by the signal source passes through the power amplifier to drive the vibration table to generate a large sensed signal.When adding a large signal, the response of the system is as shown in the Fig. 10 below.

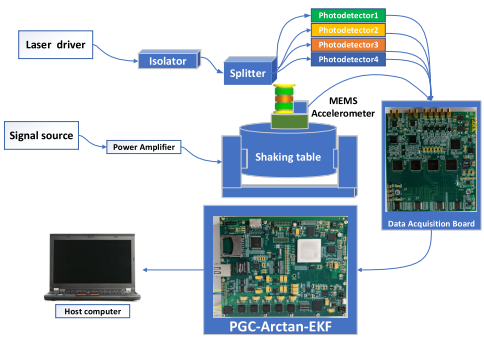

FIGURE 9. The large signal response test scheme.

As shown in Figure 10 above,the Fig.10(a) is the time domain waveform output when adding a large signal, and the Fig. 10(b) is the corresponding power spectral density waveform using 10-second datas. The THD of demodulated output signals at 220Hz can be calculated from the following

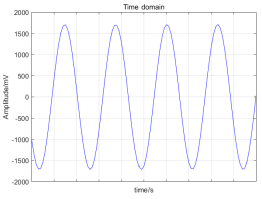

(a) The time domain waveform

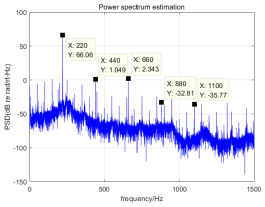

(b) The corresponding power spectral density waveform

FIGURE 10. Large signal response.

equation (16)

$$10*\log_{10}((10^{f_2/10}+10^{f_3/10}+10^{f_4/10}+10^{f_5/10})/10^{f_1/10}) \tag{27}$$

where f_1 andf_2,f_3,f_4,f_5 refer to the phase spectral density of the fundamental frequency and each harmonic, respectively, and the THD is −61.22 dB. This shows that the system has a good large signal response performance.

E. CHANNEL CROSSTALK

Channel crosstalk is the coupling between two channels that cause noise between channels. This is an undesired energy value produced by coupling one channel to another. By adding a signal to only one channel, the crosstalk of the signal to the other three signals can be observed, as shown in Figure 11.

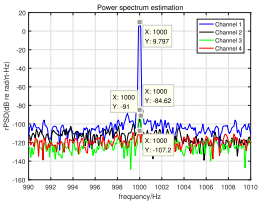

(a) Crosstalk of channel 1 to other channels

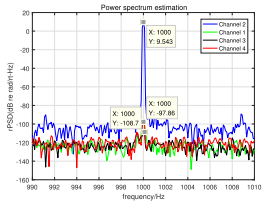

(b) Crosstalk of channel 2 to other channels

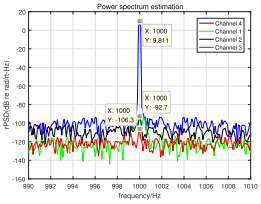

(c) Crosstalk of channel 3 to other channels

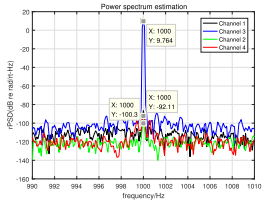

(d) Crosstalk of channel 4 to other channels

FIGURE 11. Channel crosstalk test.

It can be seen that the overall channel crosstalk of the system is better than 94dB,so there is no obvious crosstalk between the channels.

V. CONCLUSION

In this paper, we propose a new algorithm based on the traditional PGC demodulation algorithm. The algorithm has been verified both in theory and simulation.We design the optical

path and circuit,and the algorithm is implemented on hardware. In order to ensure the effectiveness of the algorithm, several experiments were carried out. It can be seen from the experimental results that PGC-Arctan-EKF guarantees that the data used in the ellipse fitting is the appropriate data, which suppresses the adverse effects caused by external disturbance on the ellipse fitting and ensures the sensitivity of the system. At the same time, the phase self-noise of the system is better than -115 dB re rad /$\mathrm{Hz}^{1/2}$, and the large signal can reach 66 dB re rad/$\mathrm{Hz}^{1/2}$ @220Hz with the THD is -61.22 dB.This shows that the system has both high sensitivity and wide dynamic range.

REFERENCES

[1] Y. Shindo, T. Yoshikawa, and H. Mikada, "A large scale seismic sensing array on the seafloor with fiber optic accelerometers," in *Proc. IEEE SENSORS*, vol. 2, Jun. 2002, pp. 1767–1770.

[2] A. Abdallah, "Experimental study on an interferometric strain sensor based on hollow-core photonic bandgap fiber for intrusion detection," *Opt. Commun.*, vol. 428, pp. 35–40, Dec. 2018.

[3] B. Culshaw and A. Kersey, "Fiber-optic sensing: A historical perspective," *J. Lightw. Technol.*, vol. 26, no. 9, pp. 1064–1078, May 1, 2008.

[4] K. S. Sham, C. V. Sreehari, K. Vivek, T. V. Praveen, K. P. B. Moosad, and R. Rajesh, "Experimental investigations on implementing different PGC algorithms for interrogation of fiber optic hydrophones," *Proc. SPIE*, vol. 9654, Jun. 2015, Art. no. 96542A.

[5] T. G. Giallorenzi, J. A. Bucaro, A. Dandridge, G. H. Sigel, J. H. Cole, S. C. Rashleigh, and R. G. Priest, "Optical fiber sensor technology," *IEEE Trans. Microw. Theory Techn.*, vol. 30, no. 4, pp. 472–511, Apr. 1982.

[6] M. Liu, T. Song, and G. Gui, "Deep cognitive perspective: Resource allocation for NOMA-based heterogeneous IoT with imperfect SIC," *IEEE Internet Things J.*, vol. 6, no. 2, pp. 2885–2894, Apr. 2019.

[7] G. Gui, H. Huang, Y. Song, and H. Sari, "An effective NOMA scheme based on deep learning," *IEEE Trans. Veh. Technol.*, vol. 67, no. 9, pp. 8440–8450, Sep. 2018.

[8] J. Pan, Y. Yin, J. Xiong, W. Luo, G. Gui, and H. Sari, "Deep learning-based unmanned surveillance systems for observing water levels," *IEEE Access*, vol. 6, pp. 73561–73571, 2018.

[9] Y. Tu, Y. Lin, J. Wang, and J.-U. Kim, "Semi-supervised learning with generative adversarial networks on digital signal modulation classification," *Comput. Mater. Continua*, vol. 55, no. 2, pp. 243–254, 2018.

[10] P. Wang, G. Brambilla, M. Ding, Y. Semenova, Q. Wu, and G. Farrell, "High-sensitivity, evanescent field refractometric sensor based on a tapered, multimode fiber interference," *Opt. Lett.*, vol. 36, no. 12, pp. 2233–2235, Jun. 2011.

[11] T. Jiao, H. Meng, S. Deng, S. Liu, X. Wang, Z. Wei, F. Wang, C. Tan, and X. Huang, "Simultaneous measurement of refractive index and temperature using a Mach-Zehnder interferometer with forward core-cladding-core recoupling," *Opt. Laser Technol.*, vol. 111, pp. 612–615, Apr. 2019.

[12] A. Dandridge, A. Tveten, and T. Giallorenzi, "Homodyne demodulation scheme for fiber optic sensors using phase generated carrier," *IEEE J. Quantum Electron.*, vol. JQE-18, no. 10, pp. 1647–1653, Oct. 1982.

[13] A. Zhang and S. Zhang, "High stability fiber-optics sensors with an improved PGC demodulation algorithm," *IEEE Sensors J.*, vol. 16, no. 21, pp. 7681–7684, Nov. 2016.

[14] Y. Lin, H. Tao, Y. Tu, and T. Liu, "A node self-localization algorithm with a mobile anchor node in underwater acoustic sensor networks," *IEEE Access*, vol. 7, pp. 43773–43780, 2019.

[15] S. Wang, Y. Lin, H. Tao, P. K. Sharma, and J. Wang, "Underwater acoustic sensor networks node localization based on compressive sensing in water hydrology," *Sensors*, vol. 19, no. 20, p. 4552, Oct. 2019.

[16] Y. Lin, X. Zhu, Z. Zheng, Z. Dou, and R. Zhou, "The individual identification method of wireless device based on dimensionality reduction and machine learning," *J. Supercomput.*, vol. 75, no. 6, pp. 3010–3027, Jun. 2019.

[17] H. Wang, J. Li, L. Guo, Z. Dou, Y. Lin, and R. Zhou, "Fractal complexity-based feature extraction algorithm of communication signals," *Fractals*, vol. 25, no. 04, Aug. 2017, Art. no. 1740008.

[18] G. Gui, H. Sari, and E. Biglieri, "A new definition of fairness for non-orthogonal multiple access," *IEEE Commun. Lett.*, vol. 23, no. 7, pp. 1267–1271, Jul. 2019.

[19] G. Gui, H. Huang, Y. Song, and H. Sari, "Deep learning for an effective nonorthogonal multiple access scheme," *IEEE Trans. Veh. Technol.*, vol. 67, no. 9, pp. 8440–8450, Sep. 2018.

[20] G.-Q. Wang, T.-W. Xu, and F. Li, "PGC demodulation technique with high stability and low harmonic distortion," *IEEE Photon. Technol. Lett.*, vol. 24, no. 23, pp. 2093–2096, Dec. 1, 2012.

[21] X. Yang, Z. Chen, J. H. Ng, V. Pallayil, and C. K. C. Unnikrishnan, "A PGC demodulation based on differential-cross-multiplying (DCM) and arctangent (ATAN) algorithm with low harmonic distortion and high stability," *Proc. SPIE*, vol. 8421, Oct. 2012, Art. no. 84215J.

[22] Y. Tong, H. Zeng, L. Li, and Y. Zhou, "Improved phase generated carrier demodulation algorithm for eliminating light intensity disturbance and phase modulation amplitude variation," *Appl. Opt.*, vol. 51, no. 29, pp. 6962–6967, Oct. 2012.

[23] H. Wang, L. Guo, Z. Dou, and Y. Lin, "A new method of cognitive signal recognition based on hybrid information entropy and D-S evidence theory," *Mobile Netw. Appl.*, vol. 23, no. 4, pp. 677–685, Aug. 2018.

[24] Y. Li, Y. Lin, X. Cheng, Z. Xiao, F. Shu, and G. Gui, "Nonconvex penalized regularization for robust sparse recovery in the presence of α noise," *IEEE Access*, vol. 6, pp. 25474–25485, 2018.

[25] Y. Zhang, J. Ning, S. Yang, and H.-L. Cui, "Field test investigation of fiber optic seismic geophone in oilfield exploration," *Proc. SPIE*, vol. 6770, Oct. 2007, Art. no. 677005.

[26] J. Han, W. Zhang, D. Jiang, Z. Wang, and F. Li, "Fiber optic 3-component seismometer," *Photon. Sensors*, vol. 4, no. 2, pp. 102–107, Jun. 2014.

[27] B. Wu, Y. Yuan, J. Yang, A. Zhou, and L. Yuan, "Improved signal demodulation method in optical fiber seismometer," *Sensor Lett.*, vol. 10, no. 7, pp. 1400–1404, Jul. 2012.

[28] Q. Shi, "Performance improvement of phase-generated carrier method by eliminating laser-intensity modulation for optical seismometer," *Opt. Eng.*, vol. 49, no. 2, Feb. 2010, Art. no. 024402.

[29] J. He, L. Wang, F. Li, and Y. Liu, "An ameliorated phase generated carrier demodulation algorithm with low harmonic distortion and high stability," *J. Lightw. Technol.*, vol. 28, no. 22, pp. 3258–3265, Nov. 15, 2010.

[30] A. Zhang and D. Li, "Interferometric sensor with a PGC-AD-DSM demodulation algorithm insensitive to phase modulation depth and light intensity disturbance," *Appl. Opt.*, vol. 57, no. 27, pp. 7950–7955, Sep. 2018.

[31] J. Chen, W. Gao, T. Chang, W. Sun, Z. Wang, M. Yu, Y. Yang, Q. Fu, and H.-L. Cui, "Method for determining the resonance frequency of a fiber optic interferometric accelerometer," *IEEE Trans. Instrum. Meas.*, vol. 67, no. 3, pp. 698–705, Mar. 2018.

[32] J. Chen, T. Chang, Q. Fu, J. Lang, W. Gao, Z. Wang, M. Yu, Y. Zhang, and H.-L. Cui, "A fiber-optic interferometric tri-component geophone for ocean floor seismic monitoring," *Sensors*, vol. 17, no. 12, p. 47, Dec. 2016.

[33] C. Ni, M. Zhang, Y. Zhu, C. Hu, S. Ding, and Z. Jia, "Sinusoidal phase-modulating interferometer with ellipse fitting and a correction method," *Appl. Opt.*, vol. 56, no. 13, pp. 3895–3899, May 2017.

CHANGBO HOU received the B.S. and M.S. degrees from the College of Information and Communication Engineering, Harbin Engineering University, Heilongjiang, China, in 2008 and 2011, respectively, where he is currently pursuing the Ph.D. degree with the Key Laboratory of In-ber Integrated Optics, Ministry Education, China. He is currently a Lecturer with the College of Information and Communication Engineering, Harbin Engineering University. His research interests include wideband signal processing, optical sensors, image processing, and deep learning.

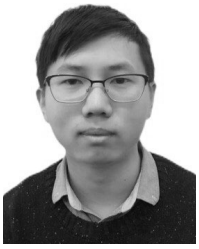

GUOWEI LIU received the B.S. degree in electronic information engineering from Harbin Engineering University, Heilongjiang, China, in 2019. His research interests include edge computing, deep learning, and signal processing.

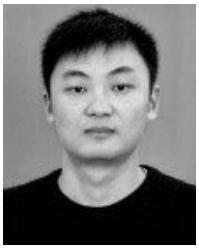

SHUAI GUO received the B.S. degree from the College of Information and Communication Engineering, Harbin Engineering University, Heilongjiang, China, in 2017. He is currently pursuing the M.S. degree with the College of Information and Communication Engineering, Harbin Engineering University. His research interests include signal processing, parameter estimation, and the demodulation algorithms of optical fiber sensors.

SHUAIFEI TIAN received the B.Eng. degree in optoelectronic materials and devices from Harbin Engineering University, Harbin, China, in 2016, where he is currently pursuing the Ph.D. degree in optical engineering. His current research interest includes fiber-optic interferometers.

YONGGUI YUAN is currently with the Key Laboratory of In-fiber Integrated Optics, Ministry Education of China, Harbin Engineering University, Harbin, China, and also with the College of Physics and Optoelectronic Engineering, Harbin Engineering University.